ChemPubSoc Europe

DOI: 10.1002/cphc.201700725

CHEMPHYSCHEM Articles

Water Dynamics and Proton-Transport Mechanisms of Nafion 117/Phosphotungstic Acid Composite Membrane: A Molecular Dynamics Study

Saeed Akbari,[a] Mohammad Taghi Hamed Mosavian,*[a] Ali Ahmadpour,[a] and Fatemeh Moosavi[b]

The use of a Nafion/phosphotungstic acid composite membrane and the impact of varying concentration of heteropoly acid (HPA) on the well-known effective mechanisms of proton transport were investigated by using classical and quantum hopping molecular dynamics simulation. Our simulations demonstrated that the HPA particles have a favorable influence on the Grotthuss mechanism in proton transportation at low hydration levels. From radial distribution function examinations, it was found that HPA particles were solvated with water and also exhibited stronger affinity toward hydronium ions. It can be concluded that addition of hydrophilic particles such as HPA improved proton conductivity. To assess this effectiveness, lifetime and half-life of the hydrogen bond (H-bond) network in the formed water clusters were investigated at different HPA concentrations. The analysis of H-bond network stability revealed that the lifetime of H-bonds between water molecules and protons decreased with increasing HPA concentration. Moreover, we found that the H-bond network between water molecules was more stable, and the mismatch between simulated bulk water and those formed water clusters in the considered systems decreased upon HPA addition. Indeed, for HPA doped membrane, the activation energy of proton transfer process from a hydronium ion to a water molecule was lower than for the undoped system. The water diffusion coefficient decreased and that of the hydronium ion enhanced with an increase in HPA doping level.

1. Introduction

Over the last decade, polymer electrolyte fuel cell (PEFC) systems have been considered a promising energy source to substitute fossil energy because of their high efficiency and low pollution. PEFCs directly convert the chemical energy of fuel into electrical energy, in which the protons, as a product of hydrogen oxidation reaction (HOR) at the anode chamber, permeate through a proton exchange membrane (PEM) to form water by the oxygen reduction reaction (ORR) at the cathode chamber.[1,2]

Among the large family of perfluorosulfonic acid (PFSA) polymers, Nafion is noteworthy for its excellent conductivity and exceptional chemical, thermal, and mechanical stability.[3,4] PEMs are known to be a key component of PEFCs. Adequate water saturation is recognized as an integral part of PEM and it plays a vital role in practical proton conductivity.

To prevent anode-catalyst poisoning by CO and to improve the kinetics of fuel oxidation, the PEFCs can be operated at higher temperatures (above 80 °C).[5,6] Due to the lack of water retention at elevated temperature operation, the proton conductivity of PEMs is still unsatisfactory. Therefore, it is an important and challenging task to develop an appropriate membrane that offers both suitable water uptake and high proton conductivity for PEFC applications.

To improve the proton-conducting characteristics of PEMs, inorganic superacids, for example, heteropoly acids (HPA) and zirconium phosphonate, have been incorporated into the membrane, developing a composite polymer electrolyte.[7–12] Remarkably, the exceptional ionic conductivity, as well as the ability of HPA to increase local proton concentration, afford potential applications as doping agents to enhance the conductivity of PEMs under drier conditions.[13]

An example of a well-known structure of HPA is the α-Keggin with the general formula $[XM_{12}O_{40}]^{n-}$, where X indicates the heteroatom, which is usually a main-group element (P, Si, Al, etc.) and M represents the addenda atoms, which are commonly tungsten or molybdenum elements (Figure 1).[14] Phosphotungstic acid $[H_3PW_{12}O_{40}]$ (hereafter noted PW_{12}) has been the subject of intensive experimental studies as, for instance, an inorganic additive for PFSA membrane.[8,15–18] Malhotra et al.[19] have investigated Nafion 117 impregnated with HPA particles and obtained a dramatic improvement in fuel cell output for composite film as compared with pure ionomer film. Ramani et al.[16] have studied Nafion/HPA composite film with various concentration of HPA in the fuel cell. They concluded that the proton conductivity and thermal stability of Nafion improve because of HPA addition. The authors also reported that the water uptake of HPA doped Nafion was greater

[a] S. Akbari, Prof. M. T. H. Mosavian, Prof. A. Ahmadpour
Chemical Engineering Department
Faculty of Engineering
Ferdowsi University of Mashhad (Iran)
E-mail: mosavian@um.ac.ir

[b] Dr. F. Moosavi
Department of Chemistry
Faculty of Science, Ferdows
University of Mashhad (Iran)

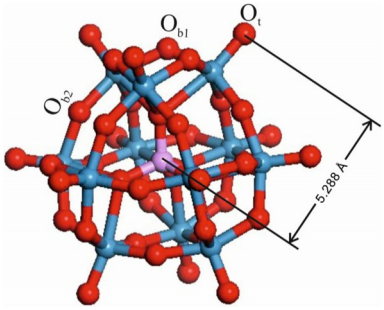

Figure 1. The simulated α-Keggin $[PW_{12}O_{40}]^{3-}$ anion and definition of terminal O_t and bridging O_{b1} oxygen atoms.

than for the undoped film at high temperatures. However, details of how the improved performance of the membrane by such hydrophilic particles is brought about must be investigated.

To our knowledge, vehicular and Grotthuss mechanisms are the two predominant mechanisms that establish the characteristics of proton conduction for PEM through hydrophilic domains. The self-diffusion coefficient of the vehicle (in this case, water) is determinative in the rate of proton transfer through a vehicular mechanism. On the other hand, a full understanding of the Grotthuss mechanism requires a deep analysis of hydrogen-bonding networks.[20]

More recently, an experimental and theoretical study of 3 M ionomer containing PW_{12} was conducted by Liu et al.[21] In fact, they performed PGSE-NMR spectroscopy to obtain the diffusion coefficient of water molecules with different hydration levels in 3 M ionomers. When ionic conductivity of the membrane was measured and the Nernst–Einstein equation was used, the discrepancy between measured and calculated conductivity was assigned to the impact of Grotthuss hopping on proton transportation. In addition, they conclude that the higher ionic conductivity of composite membrane at higher doping levels is due to Grotthuss hopping mechanism improved by PW_{12} anions. However, no detailed molecular-level understanding of the mechanism has been provided.

To our knowledge, in both experimental and theoretical studies,[8,15,19,21,22] there seems to be a common consensus about the domination of the Grotthuss mechanism when the PFSA is doped with HPAs, but no definitive proof is available. Clarifying the molecular details of how this dopant enhances ionic conductivity is not easy with current experimental techniques; nevertheless, theoretical and computational studies such as molecular dynamics (MD) simulations and ab initio computations can be used to directly probe the proton dynamics and provide more quantitative information about the transportation mechanism. One of the prerequisites for proton transport through the Grotthuss mechanism is H-bond breaking and forming, and ab initio MD simulation would capture this process. The multistate empirical valence bond (MS-EVB) method[23,24] and the recently developed self-consistent MS-EVB (SCI-MS-EVB) methodology[25] are particular versions of reactive MD for determining the mechanisms affecting proton transport in PFSA membranes. Likewise, the quantum hopping (Q-HOP) MD method has been somewhat successful in describing the proton transport process. This method is frequently used to study dynamic proton equilibria in condensed phases.[26–28] Groot et al.[29] performed Q-HOP simulations for Aquaporin-1 to study the mechanism of proton exclusion. More recently, Devanathan et al.[30] investigated proton hopping in PEMs by using the Q-HOP MD method. They characterize the intrinsic nature of the hydrated excess protons in hydrophilic Nafion domains. In principle, Q-HOP MD can be applied to many different systems such as protein and polymer systems because of its general parameterization scheme, and simulation of large systems for longer time periods (i.e. several nanoseconds) is feasible with this method.

In this study, the impact of PW_{12} on some of the requirements of Grotthuss and vehicular mechanisms inside the Nafion 117 will be investigated by using classical and Q-HOP MD simulations. Analysis of the static features and transport dynamics is also performed, together with a detailed investigation of the hydrogen bond networks. Furthermore, the diffusivity of hydronium ions and water for Nafion/PW_{12} composite membranes with different doping levels is studied for various water contents. The global aim of this study is to explore the effect of HPA on membrane properties and to provide a definitive proof for previous experimental studies on HPA doped PFSA membranes.

2. Simulation Details

2.1. Classical MD Simulations

Nafion polymer chains include two components: the backbone and the side chain. The former constitutes the hydrophobic domain, and the latter forms the hydrophilic domain of the membrane. Figure 2 shows the chemical structure of the Nafion monomer with EW = 1148 employed in the present study. The ratio of the weight of Nafion (in terms of molecular mass) to sulfonic acid group is defined as equivalent weight (EW).

The simulation cubic boxes contain 40 polymer chains (400 SO_3^-) located randomly in the box. Each chain consists of 682 atoms, with an F atom at each end. To investigate the influence of adding PW_{12} on the structural and dynamical properties of Nafion, the systems were approximately doped with 0, 2, 8, and 15 wt% PW_{12}. The water molecules were then added.

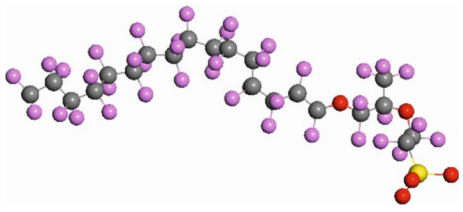

Figure 2. Chemical structure of Nafion 117 used in the present study (C atoms in gray; F atoms in purple; O atoms in red; and S atom in yellow).

Based on the study of Paddison and Elliott,[31] all sulfonate groups for $\lambda \geq 3$ are ionized by protons in the form of H_3O^+. The λ parameter is defined as the ratio of water molecule number to number of SO_3^- groups.[32] The membrane was solvated by water contents of $\lambda = 1$, 3, 5, 7, 12, and 20. It is worth mentioning that, according to the ab initio modeling results of Paddison and Elliott[31] and the limitations on the proton transfer from sulfonic groups to water at $\lambda = 1$, this value of λ is merely considered for investigating a classical benchmark.

The DREIDING force field recently modified by Mabuchi et al.[33] was used for the fluorocarbon part and the torsion potentials for Nafion. The partial charges for Nafion and the classical hydronium model for hydronium ions were taken from Jang et al.[32] Given that PFSA ionomers are macromolecules, the flexible three-centered (F3C) model was applied to describe water molecules.[34]

Prior to the MD simulations, the PW_{12} molecule was optimized by using Gaussian 09[35] software, and the ChelpG method[36] was used to assign partial charges. For this purpose, DFT calculations at the B3LYP/LANL2DZ level of theory were performed.

The force field parameters for PW_{12} were taken from Ref. [37]. To calculate the intermolecular interactions, the Lorentz–Berthelot mixing rules, $\sigma_{ij} = 1/2(\sigma_i + \sigma_j)$ and $\varepsilon_{ij} = (\varepsilon_i \varepsilon_j)^{1/2}$, were implemented.

In addition to the separate minimization of each system by using the steepest descent algorithm,[38] the following steps were implemented to obtain the initial structures and thus final density at each hydration level: 1) NPT MD simulation with $T = 600$ K and $P = 1$ MPa. It should be noted that the value of ε for Nafion is reduced to 1/100 magnitude at this step. 2) NPT MD simulation in which the Lennard–Jones (LJ) potential parameters were returned to the normal values at $T = 300$ K and $P = 101.325$ kPa for 100 ps. 3) NPT MD simulations with temperature variation between 300 K and 600 K and $P = 101.325$ kPa for 250 ps. This step was repeated four times. 4) Equilibrium NPT MD simulation at $T = 300$ K and $P = 101.325$ kPa for 300 ps. For each water content, the simulation density was calculated when the system reached stable equilibration.

To compare the results with respect to density, the experimental correlation with λ proposed by Morris and Sun[39] was applied. They estimated the experimental density of the membrane (EW = 1148) using Equation (1):

$$\rho\left(\frac{g}{cm^3}\right) = \frac{63.7 + \lambda}{31.1 + \lambda} \quad (1)$$

The leapfrog algorithm[40] was used for integration of the equations of motion with timestep 1 fs. The production run within the canonical ensemble (NVT) was carried out for 2 ns at 300 K and 1 atm for each λ, and the trajectory of molecules was collected every 0.1 ps (20 000 configurations). All the MD simulations were conducted using the DL_POLY package[41] with periodic boundary conditions and cutoff distance of 15 Å for the Coulomb potential. The pressure was maintained constant by using Berendsen barostat[42] and the Nosé–Hoover thermostat[43] for temperature control was applied.

Long-range electrostatic interactions were computed by using the Ewald summation method[44] with a tolerance factor 1×10^{-6} (known as Ewald sum precision). Scheme 1 represents the simulation procedure step by step.

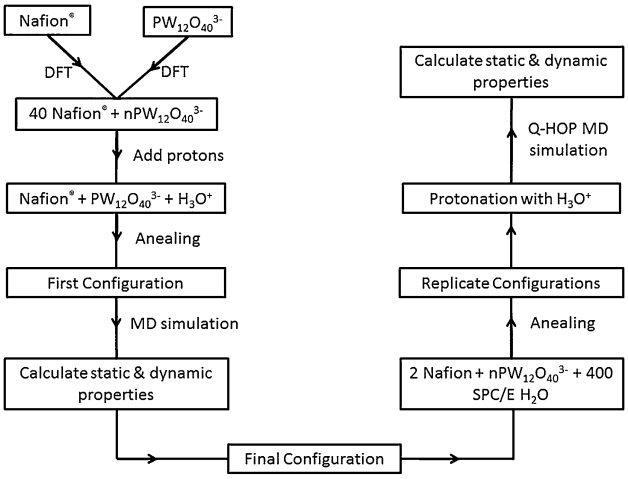

Scheme 1. The stepwise simulation procedure.

2.2. Q-HOP MD Simulation

Given that classical MD simulations are not suitable for directly probing the hopping mechanism of proton transport, further particular simulations had to be made using theoretical approaches that incorporate quantum chemical methods into MD simulations. In the present work, the Grotthuss mechanism in proton transport process was studied by using Q-HOP MD simulation. To construct a favorable configuration for the Q-HOP MD simulation, three model systems were produced using final configuration from classical MD simulations. Two Nafion chains (20 SO_3^-), 26 H_3O^+ ions, 2 PW_{12} particles, and 400 SPC/E[45] H_2O molecules were initially annealed by using the annealing procedure as described in Section 2.1. To create the input configuration for the Q-HOP MD simulation, the implemented procedure described by Devanathan et al.[30] was used. The final systems contained 8, 4, and 2 PW_{12}, which corresponds to approximately 15.7, 8.5, and 2.5 wt%, respectively. All the simulations were carried out with NWCHEM[46,47] code and the AMBER 99/GAFF[48,49] force field was used. It should be noted that the general features of Nafion morphology and H_2O/H_3O^+ transport is essentially independent of force fields and codes used.[30] The cutoff distance for non-bond interactions was 10 Å and the Particle Mesh Ewald (PME)[44] method was used to calculate long-range electrostatic interactions. The equations of motion were solved by using the leapfrog Verlet[40] algorithm with a time step of 1 fs. After 200 ps equilibration run, 2 ns production run was performed using the NPT ensemble at 300 K. Scanning for proton transport events was carried out every 10 steps and the trajectories and proton transfer information were also recorded to track all hopping events.

3. Results and Discussion

The experimental and simulation densities at each λ for undoped Nafion are listed in Table 1. The differences between ρ_{exp} and ρ_{sim} were found to be less than 0.5%, except for $\lambda \leq 3$.

Table 1. Calculated density of hydrated Nafion membrane at different hydration levels. Simulation results are compared with experimental data[39] and other simulated results.

λ	ρ_{sim} [g cm^{-3}]				ρ_{exp} [g cm^{-3}>]	Box length [Å]
	Our study	Ref. [41]	Ref. [29]	Ref. [42]		
1	1.96	1.76	1.99	–	2.02	176.65
3	1.92	1.80	1.93	–	1.96	177.48
5	1.90	1.82	–	–	1.90	178.06
7	1.85	1.78	–	–	1.86	178.97
12	1.75	–	1.75	1.67	1.76	181.00
20	1.64	1.62	–	1.56	1.64	183.88

For undoped systems, the lengths of the simulation box are also listed in the last column of Table 1. After the annealing procedure, we found that each system reached a stable equilibrium and then the production runs were carried out for 2 ns. Given that we did not observe significant changes of the diffusion coefficients upon increasing the simulation length beyond 2 ns, we conclude that this length is sufficient to robustly compute diffusion coefficients of these systems.

In agreement with other studies,[34,50] by increasing water uptake, the value of calculated density gradually decreases. The density fluctuations after adding 2, 8, and 15 wt% PW_{12} are shown in Figure 3. The ρ_{sim} values for all of doped systems were larger than for the undoped systems. It can be seen that, at higher concentrations of PW_{12}, an enhancement of the calculated densities was observed. This feature might be due to morphological changes of membrane caused by the interactions between the polyoxometalate (POM) anions and polymer chains. In what follows, this issue will be discussed comprehensively.

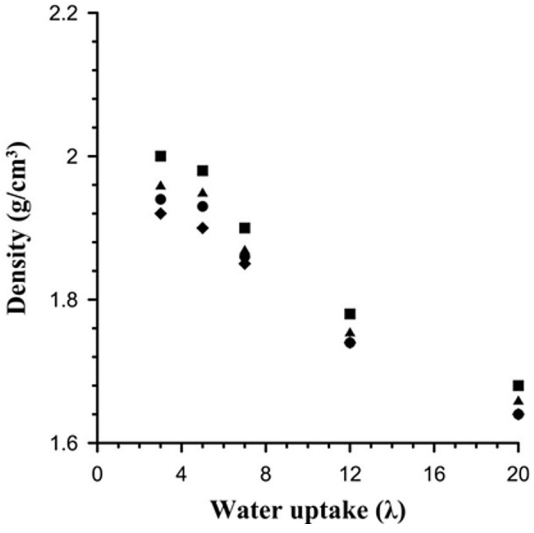

Figure 3. The simulated density of hydrated PFSA membranes as a function of hydration level (λ) (◆) 0% PW_{12} (●) 2% PW_{12} (▲) 8% PW_{12} (■) 15% PW_{12}.

3.1. Radial Distribution Function (RDF)

Pair distribution function, also known as pair correlation function, because of their spherical symmetry, represents the probability of finding atoms of A in a shell Δr at distance r of atoms of B in a system containing N particles and volume V, in accordance with Equation (2):

$$g(r)_{A-B} = \frac{\left(\frac{n_B}{4\pi r^2 \Delta r}\right)}{\left(\frac{n_B}{V}\right)} \quad (2)$$

In other words, this function displays the arrangement of one type of atom around another type of atom in spherical shell with radius of r and thickness of Δr. Indeed, the RDF curves represent quantitative information about interactions between two kinds of atoms. All RDFs are obtained from classical MD simulation.

3.1.1. *Interactions between SO_3^- and SO_3^-*

Figure 4 depicts RDF curves for sulfonic groups of the side chain; the legend indicates corresponding coordination numbers (CN). It is noticeable that by increasing λ, the separation between these groups increases (CN decreased); therefore, the broad peaks with smaller height develop (Figure 4a). Due to the progressive SO_3^- solvation by H_2O molecules, eventually at $\lambda = 20$, the first peak approximately disappeared and the second one is only observed. In an undoped membrane, these trends are in good agreement with those reported by Mabuchi et al.[33] and by Devanathan et al.[50]

Subsequent to addition of 2 wt% PW_{12}, a similar trend was observed by increasing the hydration level, while the height of the peaks dwindled. At all hydration levels, by increasing the weight percent of the anion, the peak heights continuously decrease, affected by repulsion between the charged PW_{12} anions and sulfonic groups. Due to the mediation of water molecules, especially at $\lambda > 5$, this repulsion is reduced with enhancing water content. The reduction of the height of the peak in RDFs means a decrease in the interactions between sulfonic groups. In other words, upon adding HPA, the distance between sulfonic groups increases because of electrostatic repulsion between the POM anions and the SO_3^- groups. Accordingly, the calculated density for doped systems is slightly larger than for undoped systems.

Given that PW_{12} is highly hydrophilic, water molecules accumulate around POMs, which diminishes the repulsion between sulfonic groups and PW_{12} particles, and, naturally, the height of the peaks gradually changes at higher λ values. Figures 5a–d represent snapshots of both doped and undoped membranes after 2 ns. It is immediately apparent from Panel b or Panel d that water molecules mainly surround the POM anions. Hence,

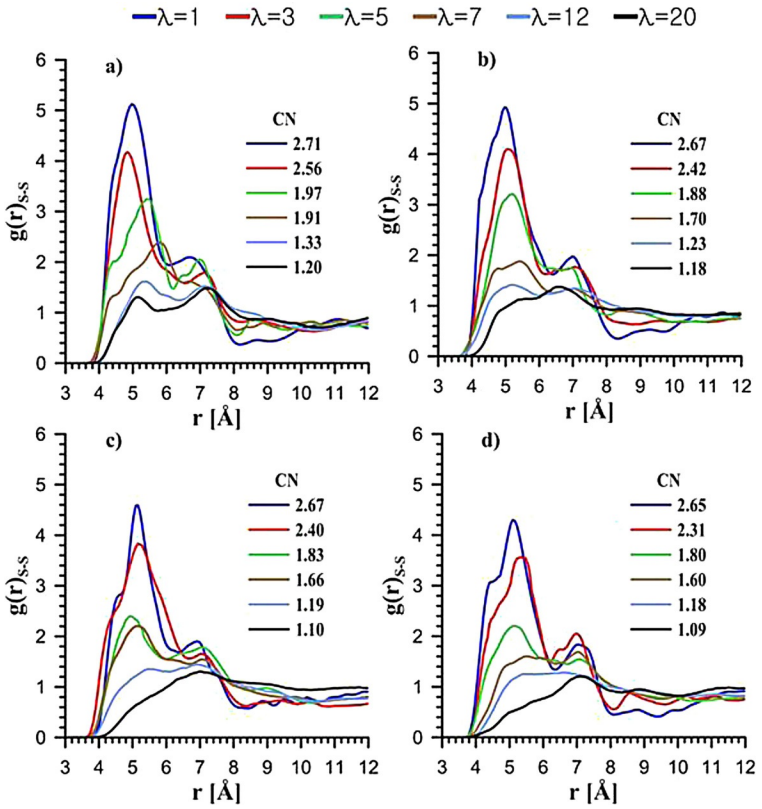

Figure 4. Radial distribution functions of a sulfur-sulfur pair at various hydration levels. a) 0% PW_{12}, b) 2% PW_{12}, c) 8% PW_{12}, d) 15% PW_{12}.

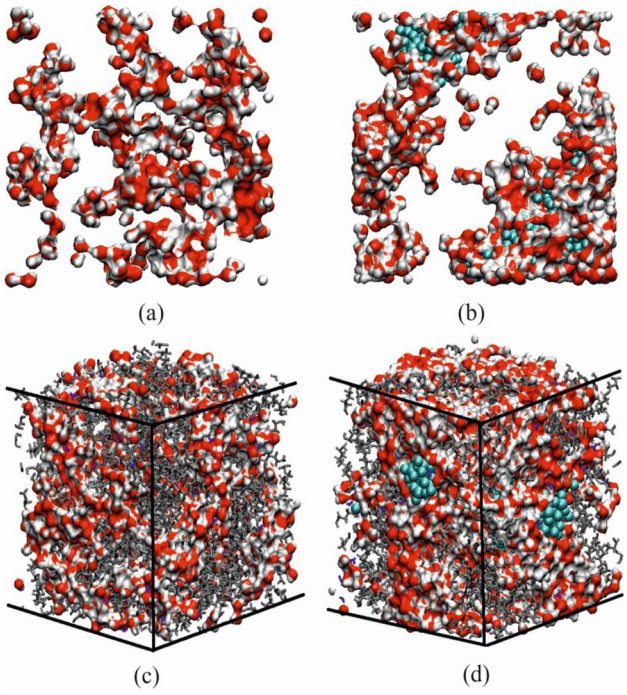

Figure 5. Snapshots of the doped and undoped membranes. Oxygen of water molecules, HPA particles, and the rest of the membrane are represented in red, cyan, and gray, respectively. a) 0% of PW_{12} at $\lambda=5$. b) 8% of PW_{12} at $\lambda=5$. c) 0% of PW_{12} at $\lambda=20$. d) 8% of PW_{12} at $\lambda=20$.

the hydrophilic character of POMs makes the formation of water clusters along the membrane more likely.

3.1.2. Interactions between SO_3^- and H_2O/H_3O^+

In Figure 6 and Figure 7 a–d, the coordination of sulfonic groups by H_2O and H_3O^+ is characterized by S-O_w RDF and S-O_h RDF, respectively (O_w, oxygen of water and O_h, oxygen of hydronium). In the case of undoped membrane, dominant peaks appear at a distance of 3.97 Å. In addition to reducing the heights, their broadening also decreases with increasing water uptake. The reduced peak heights are caused by the solvation of sulfonic groups at higher water content; in other words, the solvation of sulfonic groups increases by increasing water density. As a result, the SO_3^-–H_3O interactions decrease. The presence of water weakens the SO_3^- and H_3O^+ interactions. Such consequence can be easily implied from reductions in peak heights associated with SO_3^-–H_3O RDFs (Figure 6 a).

On the other hand, reduced peak broadenings reflect a lower number of oxygen of H_3O^+ within a sphere of radius 4.34 Å centered in a sulfur atom. The legends of plots in Figure 6 represent the CNs of H_3O^+ at first solvation shell of sulfur atoms, as discussed later.

For H_2O, the variations in the height and width of the peaks are similar to the RDFs of H_3O^+ (Figure 7 a). It should be mentioned that the area under $g(r)_{S\text{-}Ow}$ at first minimum cannot be used for calculating the CN of H_2O at first solvation shell. The number of water molecules changes from 0 to 7600, but the number of hydronium ions is constant for all the hydration levels. For this purpose, the average number of oxygen atoms from water molecules within a sphere of radius 4.5 Å of centered in sulfur atoms (first minimum of $g(r)_{S\text{-}Ow}$) was calculated from 20000 configurations. Not surprisingly, whenever the presence of water increases, not only does the CN of H_3O^+ around SO_3^- decrease, but the CN of H_2O at the first solvation shell of SO_3^- also increases.

The main object of the present study is to probe the role of HPAs in the system and the influence of the presence of POM anions. For this aim, Figure 6c–d and Figure 7 c,d, respectively, illustrate $g(r)_{S\text{-}Oh}$ and $g(r)_{S\text{-}Ow}$ at the considered concentration of PW_{12} particles. As deduced from Figure 6, the addition of POM leads to a weakening of the interactions of the sulfonic groups with hydronium ions. The decrease in the height of the peaks is an indicator of a reduction in such interactions as the doping level changes from 2 to 15 wt%. However, it should be remembered that diminishing the number of hydronium ions at first solvation shell cannot be deduced from the reduction of peak broadenings, because the number of hydronium ions in the system is not constant upon adding HPA particles.

With regard to negatively charged POM anions, it is expected that the anions attract more hydronium ions with an enhancement in concentration of HPA and thus decrease the in-

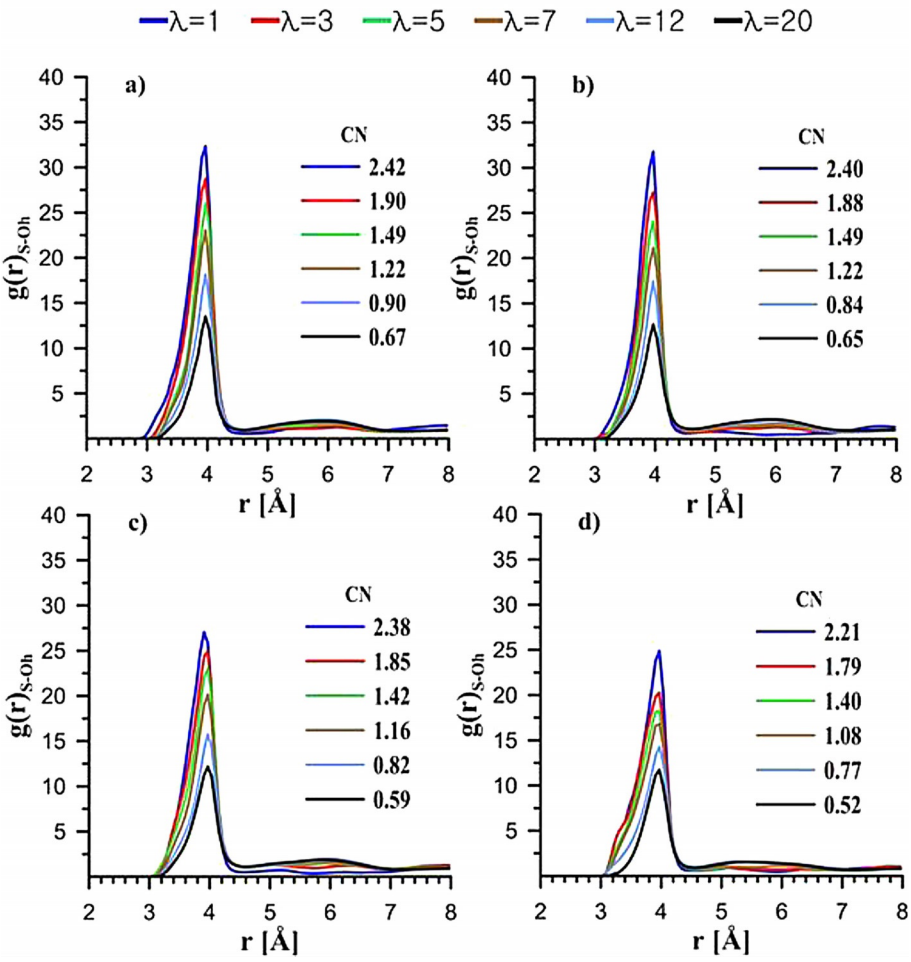

Figure 6. Radial distribution functions of sulfur-hydronium oxygen pair at various hydration levels. The coordination numbers are indicated by the legends. (a) 0% PW_{12}, (b) 2% PW_{12}, (c) 8% PW_{12}, (d) 15% PW_{12}.

teractions between SO_3^- and H_3O^+ as compared with the undoped state. This hypothesis is confirmed by RDF curves. The average number of H_2O and H_3O^+ closer than 4.34 and 4.5 Å to sulfur atoms of the SO_3^- were calculated for all considered concentrations of HPA. For example, at $\lambda \geq 3$, the CNs of the first solvating shell increase upon doping 2 wt% POM in comparison with the undoped Nafion. Under increasing concentration of POM, this descending tendency is maintained. Furthermore, the average CN of water molecules is reduced when the levels of POM doping increase. Based on the aforementioned results, generally, a higher amount of HPA in the PFSA membrane decreases the number of both H_3O^+ and H_2O in the vicinity of SO_3^-.

3.1.3. Interactions between PW_{12} and H_2O/H_3O^+

We then analyzed whether the H_3O^+ ions or H_2O molecules are pushed away from the POM anions or are more likely to be coordinated around POM anions when the PW_{12} concentration is increased. In other words, the question is how the average CNs of H_3O^+ and H_2O around POM anions change.

The most accessible atoms in POMs to interact with H_2O molecules or H_3O^+ ions are terminal oxygen atoms (O_t); toward this end, $g(r)_{Ot\text{-}Oh}$ and $g(r)_{Ot\text{-}Ow}$ are given in Figure 8. At all POM concentrations, the interactions between H_3O^+ and O_t are diminished by increasing λ, as shown in Figure 8a–c. As reported in the legend box of the figures, there will be less H_3O^+ at the first solvation shell of O_t when increasing the hydration level.

The interactions between O_t and H_2O at given hydration levels are investigated. The $g(r)_{Ot\text{-}Ow}$ represents a broad peak at distance of 2.8 Å and both heights and broadening were diminished by increasing λ (Figure 8d–f). This means that interactions between the terminal oxygen of POM and oxygen of water decrease. As reported by Chaumont et al.,[51] the interaction between POM anions and water molecules is reduced by enhancing the concentration of the anion.

In the case of the doped membrane, when the concentration of HPA increases from 2 to 15 wt%, the average O_t–O_w CN decreases at a distance of 3.2 Å from O_t (Figure 8). The interactions between O_t and O_h also decrease with increasing concentration of POM, as clearly observed in Figure 8. In other words, at specific λ, for diluted states of HPA, the interactions between cations and anions are stronger than in the case of the concentrated states of HPA, which is in good agreement with the results of Chaumont et al.[51]

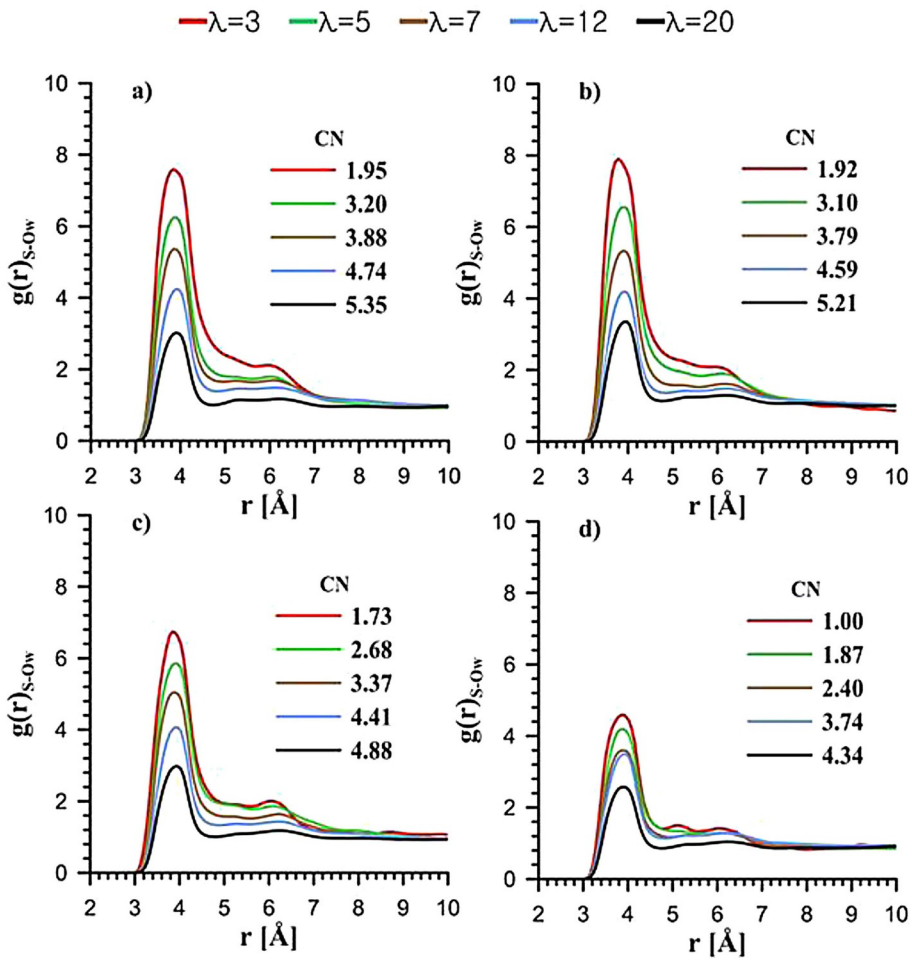

Figure 7. Radial distribution functions of sulfur-water oxygen pairs at various hydration levels. The coordination numbers are indicated in legends. a) 0% PW_{12}, b) 2% PW_{12}, c) 8% PW_{12}, d) 15% PW_{12}.

The interactions between POM and H_3O^+ are water-mediated and consequently indirect; therefore, few H-bonds will be formed between POM and H_3O^+. On the other hand, building upon the work of Lopez et al.,[37] the bridging oxygen of Type 1 of POM (O_{b1}, see Figure 1) exhibits stronger hydrogen bonds than the other ones when the MD simulation is carried out using calculated partial charges from the ChelpG method at the B3LYP/LANL2DZ level of theory.[37] Therefore, it can be concluded that the bridging oxygen of Type 1 of POM exhibits stronger interaction with water molecules in comparison with the terminal oxygen. Hence, investigating the behavior of H_3O^+ and H_2O around POM anions through the $g(r)_{Ot\text{-}Oh}$ and $g(r)_{Ot\text{-}Ow}$ is questionable. Therefore, to verify and validate the aforementioned results, the solvation of a given particle was considered. In the POM anion, the radial distance of O_t from heteroatom (P) is approximately 5.29 Å (Figure 1). Since the outermost atom of POM is O_t and the distance of the first solvation shell for O_t is 3.2 Å, we have considered the hydration of particles at a distance of 8.49 Å. The average number of coordinated H_3O^+ and H_2O around the heteroatom of the POM, namely, phosphorus, is reported in Table 2. For all the hydration levels considered, the number of coordinated water molecules around POM anions decreases by increasing weight percent of HPA and, instead, the hydronium ions are more coordinated around POM anions.

3.1.4. Interactions between H_2O and H_3O^+

In an effort to shed more light on the properties of the formed water clusters, interactions between H_2O and H_3O^+ ions have also been investigated. As expected, the interactions between H_2O and H_3O^+ decreased by increasing λ; consequently, the number of water molecules surrounding hydronium ions increases, in agreement with Devanathan et al.[50] and Cui et al.[52] (data not shown).

Next, O_w–O_h RDFs are presented in Figure 9, in which the membrane is loaded with given concentrations of HPA. The RDF curves show a sharp peak at 2.8 Å and the peak heights increase by increasing HPA concentration. It can be also found that increasing the doping level would lead to an increase in interactions between H_2O and H_3O^+.

Based on Figure 9, the first neighbor cutoff distance was chosen as 3.25 Å to calculate average CNs. It can be observed that higher HPA concentration reflects more solvation of hy-

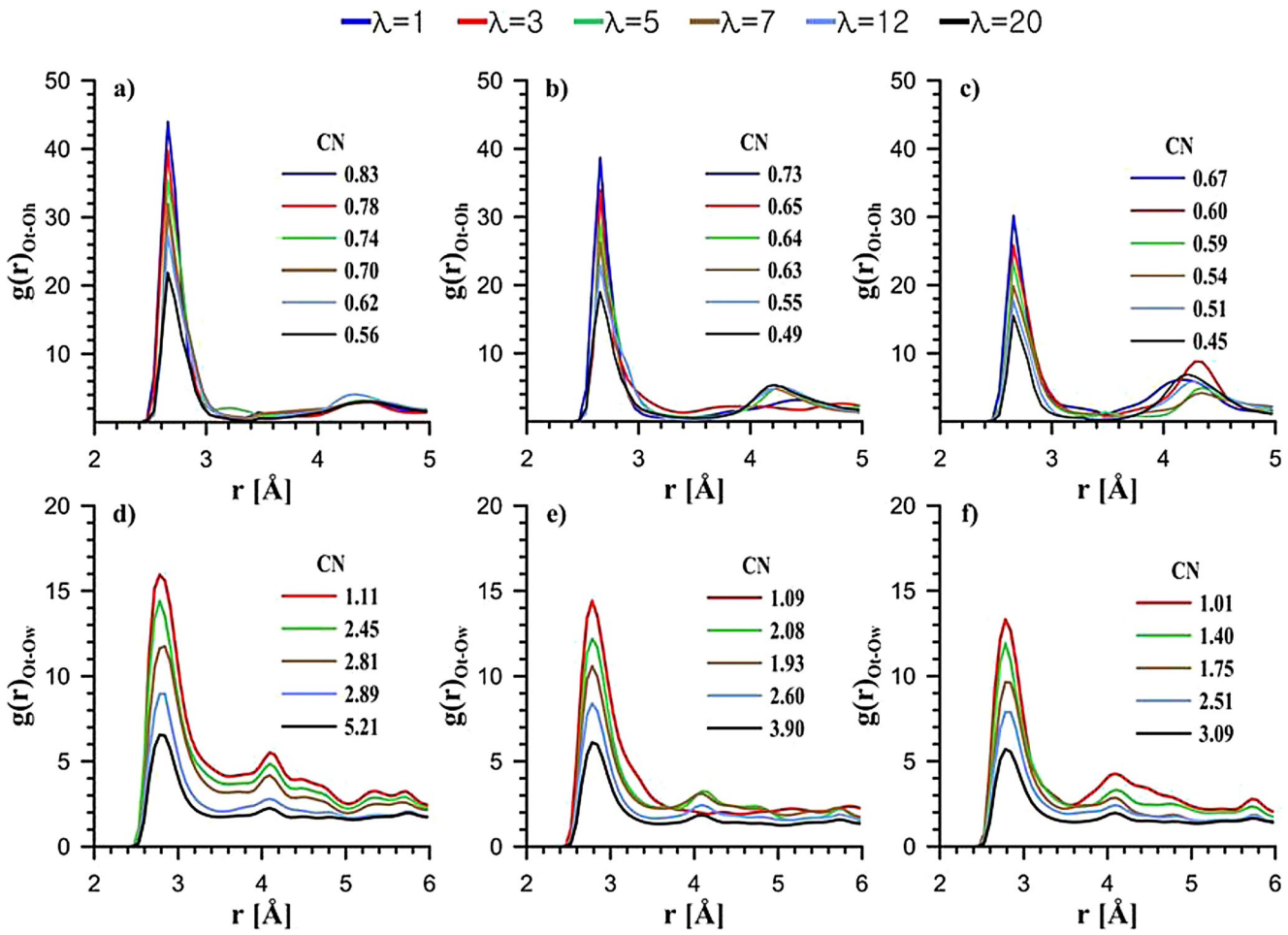

Figure 8. (top) Radial distribution functions of POM terminal oxygen-hydronium oxygen pairs at various hydration levels. a) 2% PW_{12}, b) 8% PW_{12}, c) 15% PW_{12}. (bottom) Radial distribution functions of POM terminal oxygen-water oxygen pairs at various hydration levels. d) 2% PW_{12}, e) 8% PW_{12}, f) 15% PW_{12}. The CNs are indicated by legends.

Table 2. The averaged coordination numbers (CN) of hydronium ions and water molecules around POM for systems with different HPA loadings at different hydration levels.

15 wt% H_2O	H_3O^+	8 wt% H_2O	H_3O^+	2 wt% H_2O	H_3O^+	λ
–	9.78	–	9.18	–	9.06	1
14.6	7.92	14.83	7.76	17.04	7.37	3
20.64	7.12	21.52	6.62	37.19	6.51	5
30.14	6.49	34.58	6.37	46.16	6.00	7
32.21	6.19	37.84	5.67	50.32	5.56	12
37.08	7.17	45.30	6.42	56.76	5.78	20

dronium ions, which is essential for the development of proton transport.

As noted above, because the steric hindrance of the sulfonic groups do not affect the accessibility of hydronium ions considerably, hydronium ions take part more easily in forming of hydrogen bond networks at higher doping levels. To investigate the H-bonds between protons and water molecules, the Q-HOP MD simulation was used.

3.2. Hydrogen Bonds

To investigate the dynamic behavior of H_3O^+ ions or H_2O molecules around each other, three geometrical criteria were applied, which were sufficient to analyze the lifetime of the H-bond. In the event that (i) distance between a given hydrogen bond *donor* and acceptor (all water molecules are proton acceptors) is less than 3.6 Å (the first minimum of $g(r)_{O\text{-}O}$ in pure water[53]), (ii) distance between a given hydrogen bond *donor* and hydrogen of H_3O^+ is less than 2.0 Å, and (iii) the angle ∡H-O···*donor* is less than 30°, the H-bond has been formed between a given molecule and corresponding *donor* such as water molecules.

We consider the autocorrelation function to evaluate the lifetime of an H-bond from all the trajectories (20000 configurations) of each system [Eq. (3)[42]]:

$$\tau_{HB}(t) = \frac{\langle v_{ij}(t+t_0)\cdot v_{ij}(t_0)\rangle}{v_{ij}^2(t_0)} \approx \exp\left(\frac{-t}{t_{HB}}\right) \text{ (as } t \to \infty) \qquad (3)$$

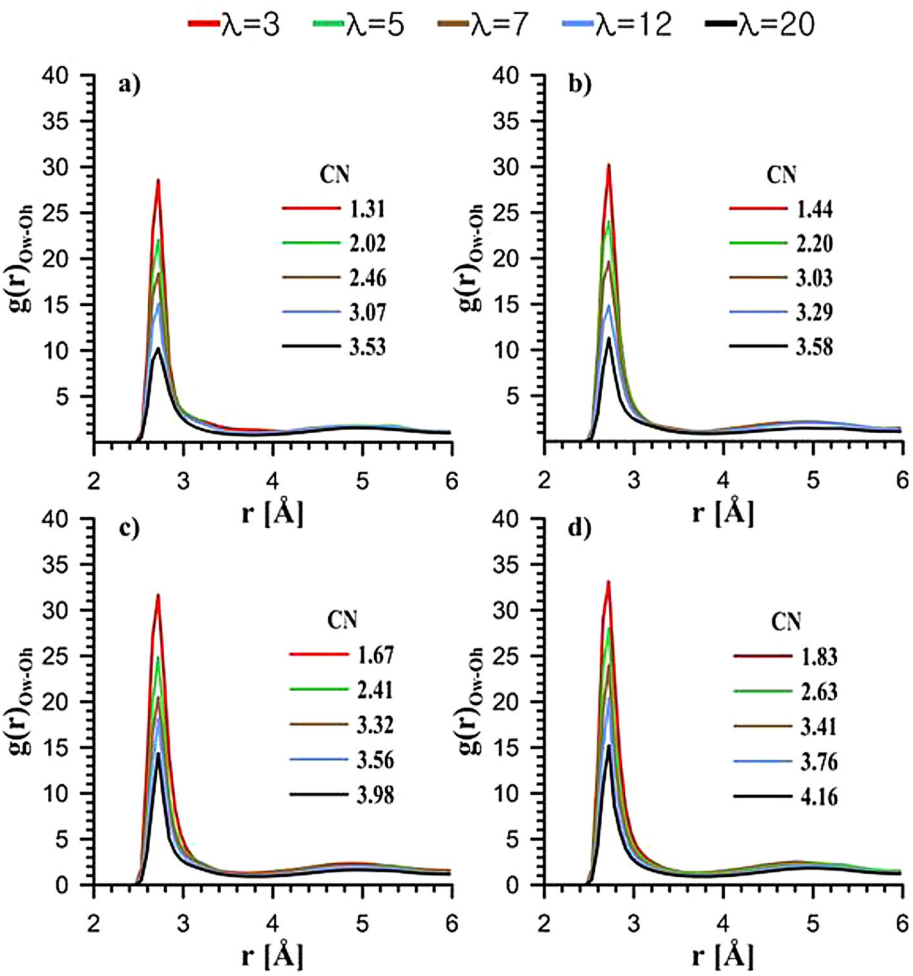

Figure 9. Radial distribution functions of water oxygen-hydronium oxygen pairs at various hydration levels. The coordination numbers are indicated in legends. a) 0% PW_{12}, b) 2% PW_{12}, c) 8% PW_{12}, d) 15% PW_{12}.

where the υ_{ij} is a Boolean variable that possesses a value of 1 if the proton resides on the *j*th acceptor site and fulfills the above three conditions at time *t*, and 0 otherwise.

Figure 10 shows the autocorrelation function $\tau_{HB}(t)$ for the relatively electronegative proton acceptor, that is, H_2O, for the case of undoped Nafion at various water content. As the figure clearly reveals, a longer persistence of the H-bond is observed between H_2O and protons under drier conditions. The lifetime and accordingly the half-life of H-bonds are reduced by increasing water content.

Persistence of H-bonds is a prerequisite of rapid proton transfer through the Grotthuss-type mechanism. Short and strong H-bonds may decrease diffusion rate and reorientation of solvent molecules.[54,55]

The strength of H-bonds is difficult to describe by using classical MD simulations, but the decrease in the lifetime of hydrogen bonds may have positive effects on proton transfer and reorientation of solvent molecules. Therefore, it can be concluded from Figure 10 that increasing the water content enhances proton transfer by the vehicular mechanism and seems to favor structural diffusion.

A similar tendency to τ_{HB} and half-life of H-bond for doped membrane was observed when compared with the undoped

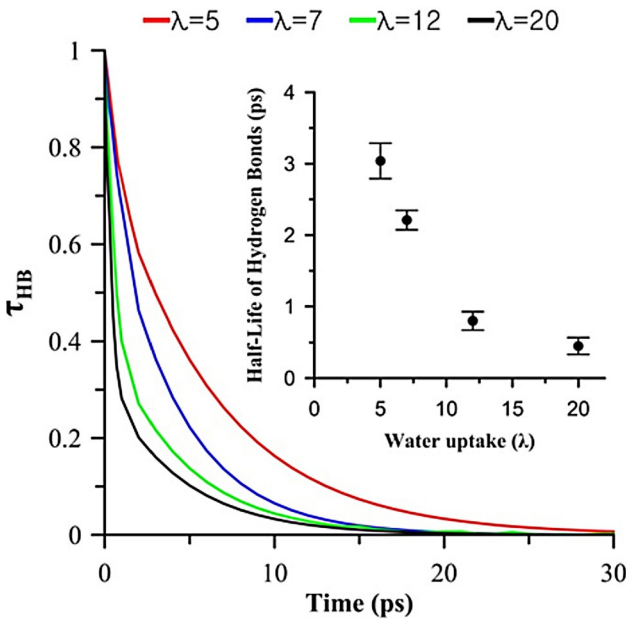

Figure 10. Lifetime of proton-water oxygen hydrogen bonds for undoped Nafion at various hydration levels. Inset represents the corresponding averaged half-life of hydrogen bonds.

state by increasing λ (the data is not shown). However, notable variations were observed for different loadings of HPA. Figure 11 illustrates τ_{HB} and the half-life of H-bond for various doping levels at $\lambda = 5$. No dramatic change was seen for either τ_{HB} or the half-life of the H-bond upon addition of 2.5 wt% HPA, whereas upon further addition of HPA (8.5 and 15.7 wt%) both τ_{HB} and the half-life of the H-bond decreased. In general, these results reveal that the structural diffusion in proton transport is more affected by higher concentration of HPA.

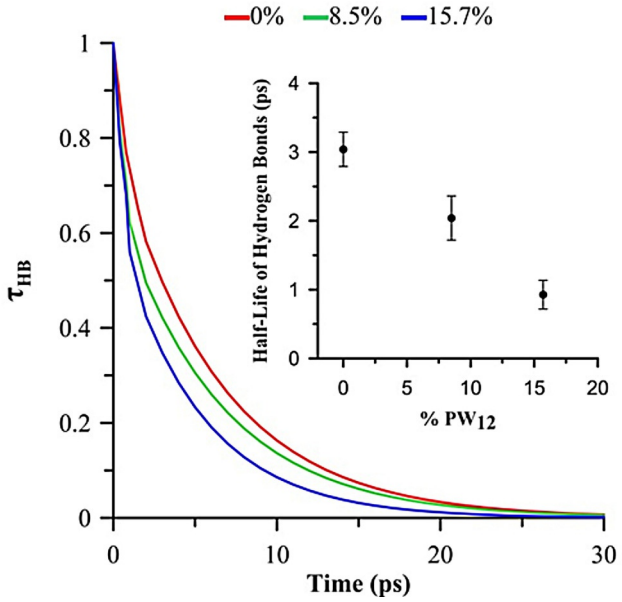

Figure 11. Lifetime of hydrogen bond of proton-water oxygen for doped Nafion at various HPA doping levels ($\lambda = 5$). The inset represents the corresponding averaged half-life of hydrogen bonds.

It is interesting to note that more H-bonds were established when POM anions exist in the membrane and the tendency of H-bond formation continues to rise by further addition of HPA.

An optimum proton conductive aqueous phase should contain moderate or weak H-bonds.[54] Actually, these particles (POMs) make the H-bond networks unstable and consequently improve proton hoping.

It is easy but wrong to deduce that these hydrophilic particles are generally added to systems as water reservoirs. In our opinion, such an explanation is not very convincing. In fact, the loosely bonded waters accumulate around HPA particles during the interaction with the surface of particles and facilitate the formation of water clusters. Then the larger water clusters enhance the mobility of water molecules and consequently the proton transfer would be sufficiently rapid through the membrane. As evidence, orthographic projections of doped and undoped Nafion at $\lambda = 5$ and $\lambda = 20$ are shown in Figure 5 visualized using VMD.[56] The accumulation of water molecules around the HPA particles is clearly depicted in Figure 5 b,d.

It is believed that the proton-hopping process occurs faster in HPA doped membrane than in undoped systems. In light of this, to evaluate the potential effects of HPA on the primary mechanism of proton transfer, the mean residence time (MRT) of the proton from τ_{HB} was calculated. Actually, MRT of the proton on a water molecule (t_{HB}) can be obtained from the slope of a linear fit to the plot of $-\ln(\tau_{HB})$ versus time.[35] Table 3 represents the calculated MRTs of the proton for all considered membranes at 300 K. The MRT decreases when λ is increased from 3 to 20. A similar observation was also obtained for the HPA doped membranes. For HPA doped membrane, the protons on average do not remain attached to water molecules for a very long time, whereas they remain for longer times in the case of the undoped membrane. Moreover, the MRT values also decrease by increasing HPA concentration at all hydration levels.

According to the relationship $k = 1/t_{HB}$, the rate constants (k) for proton hopping between water molecules are inversely related to MRTs. The values of rate constants are represented in Table 3. The experimental k for proton transfer in bulk water at 300 K is 0.63 ps^{-1}, which has been obtained by NMR techniques.[57] The rate constants increase with increasing hydration level and gradually the difference to the value reported for bulk water decreases.

Indeed, we believe that the activation energy of the process of proton transfer from H_3O^+ ions to H_2O molecules changes when the system is loaded with HPA particles. For illustration purposes, the variation of apparent activation energy was computed by using Arrhenius equation in accordance with Equation (4):

$$\frac{k_1}{k_2} = \frac{Ae^{-\frac{E_1}{RT}}}{Ae^{-\frac{E_2}{RT}}} \quad (4)$$

where E_1 corresponds to the activation energy of undoped membrane at specific λ and E_2 is the activation energy of the system with specific HPA at the same λ ($T_1 = T_2$). Given the con-

Table 3. Proton mean residence time on H_2O molecule (t_{HB}), rate constants for proton hop between water molecules (k) and variations of activation energies for Nafion with different HPA loadings at different hydration levels.

λ	t_{HB} [ps]				k [ps^{-1}]				$\Delta E = E_2 - E_1$ [kcal mol^{-1}]		
	0%	2%	8%	15%	0%	2%	8%	15%	2%	8%	15%
3	128	122	112	100	0.007	0.008	0.009	0.010	−0.03	−0.08	−0.15
5	98	87	69	60	0.010	0.012	0.014	0.017	−0.07	−0.21	−0.29
7	24	20	15	11	0.042	0.050	0.067	0.091	−0.11	−0.28	−0.47
12	5	4.5	3.3	2.9	0.200	0.222	0.303	0.345	−0.06	−0.25	−0.32
20	3	3	2.3	2.1	0.333	0.333	0.435	0.476	0.00	−0.16	−0.21

stant temperature, the difference between the levels of HPA loading ($\Delta E = E_2 - E_1$) has been reported in Table 3. For instance, at $\lambda = 5$, the activation energy 0.07 kcal mol^{-1} decreases as the membrane is loaded with 2% HPA ($\Delta E = 0.07$ kcal mol^{-1}). However, the activation energies computed at 8% and 15% doping levels decrease 0.21 and 0.29 kcal mol^{-1}, respectively; hence, a faster hopping process can be achieved at higher concentration of PW_{12}. Thus, it can be concluded that the PW_{12} particles attract the protons; meanwhile, because of the hydrophilic character, the activation energy for proton hopping process reduces in the water clusters.

3.3. Self-Diffusion Coefficients

Predictably, the presence of PW_{12} particles will affect the diffusion coefficient of the solvent molecules. Self-diffusion coefficients of hydronium ions and water were evaluated from the mean square displacement (MSD) and Einstein relationship using classical MD simulation. This procedure is in accordance with the method outlined in Ref. [58].

In practice, we can directly compare the theoretical and experimental values of the diffusion coefficient of water. Both our calculated diffusion coefficients and the experiment values (taken from Ref. [59] and Ref. [60] for hydronium ions and water, respectively) are plotted in Figure 12 (lines are drawn to show the trend). Note that D_{H_2O} increases by hydration. Closer inspection of the data demonstrates that increasing water uptake assists water diffusion. The agreement with the experimental values achieved from NMR study[59] is acceptable.

The calculated D_{H_2O} for composite membranes is consistently lower than those for the undoped membrane across the entire range of hydration; however, the general trend in diffusion coefficients was reproduced as seen in Figure 12a. This could be due to the superior propensity to retain water near HPA particles. It is clear that at the minimum hydration, HPA doped membranes exhibit a slight decrease in water diffusion coefficients and that the differences become larger as the water content increases. As discussed in Section 3.1.3, increasing the level of λ leads to additional waters to solvate the POM particles, thereby slowing the diffusion of water.

Figure 12b displays the $D_{H_3O^+}$ obtained from QENS experiments[59] together with the calculated diffusion coefficients. Due to the relative limitation of classical MD simulations in probing hydronium dynamics, a discrepancy between experimental values and simulated values is observed. Proton diffusion rate is higher in bulk water than in other water phases; hence, a similar internal structure to that of bulk water can be achieved in the hydrophilic domains as the membrane uptakes more water content.

Intuitively, one would imagine that the presence of HPA might disrupt the proton diffusion rate through negatively charged particles that attract hydronium ions; however, this point of view is not consistent with the current results. Upon more loading of HPAs, the proton diffusion, as a whole, increases at various hydration levels. For instance, the computed $D_{H_3O^+}$ increases from 3.4×10^{-7} cm^{2}s^{-1} to 6×10^{-7} cm^{2}s^{-1} at $\lambda = 5$ for 2 wt% doped membrane and 9×10^{-7} cm^{2}s^{-1} and 10.2×10^{-7} cm^{2}s^{-1} for 8%, and 15% HPA doped membranes, respectively.

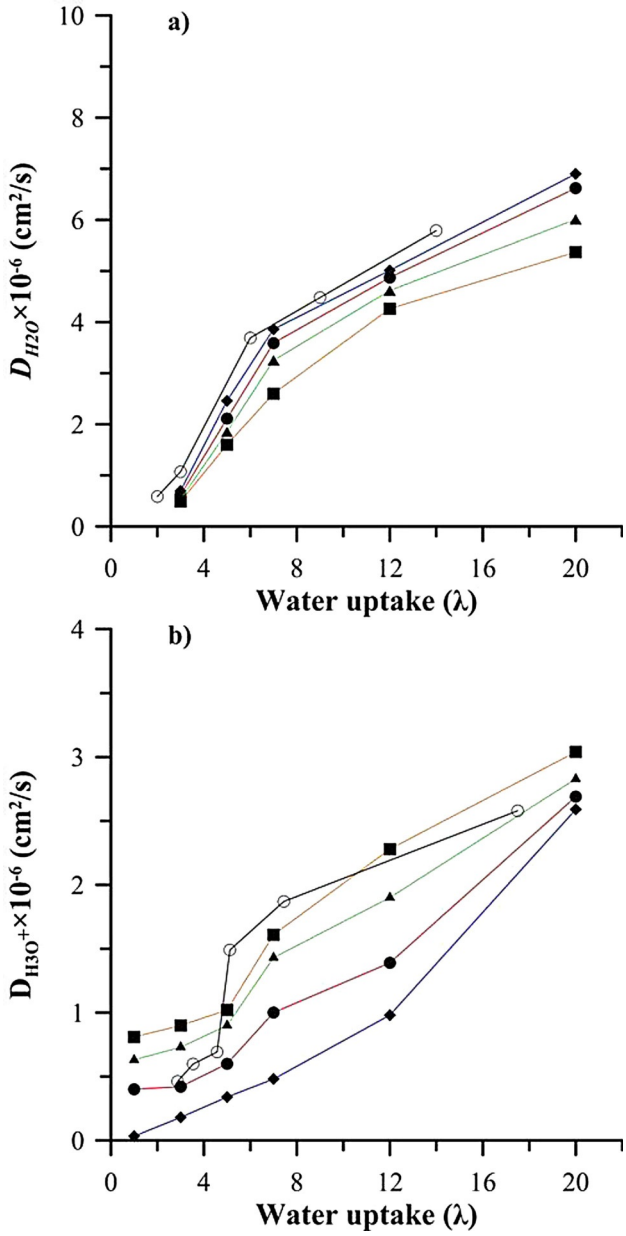

Figure 12. Variation of diffusion coefficients at different hydration levels for a) water molecules and b) hydronium ions. (○) experiment [43,44] (◆) 0% PW_{12} (●) 2% PW_{12} (▲) 8% PW_{12} (■) 15% PW_{12}.

Four water molecules surround each proton associated with HPA particles in the solid state. Two of them form a hydrogen bond between proton and water molecules and hydrogen bonding also exists between the water molecules and O_t atoms of HPA.[61] Therefore, increasing the percentage of PW_{12} could cause more hydronium ions and water molecules to cooperate in the proton transport process.

With this in mind, the variations of lifetime of the H-bonds (as discussed earlier) are hypothesized to destabilize the diffusion of hydronium ions because rapid breakup of H-bonds leads to alterations in the mobility of hydronium ions. Addi-

tionally, Herring et al.[21] addressed another possible cause based on ATR-FTIR measurements that showed easier formation of Zundel ions ($H_5O_2^+$) and Eigen ions ($H_9O_4^+$) in the hydrophilic domains brought on by the presence of HPAs. Therefore, we think that the role of the HPA in the composite membrane is to accelerate dissociation of protons by rapid cleavage of H-bonds as well as to reduce resistance of transport through hopping by facilitating the formation of Zundel and Eigen ions in hydrophilic domains.

4. Conclusions

Using classical MD and Q-HOP MD simulations, we investigated the Nafion 117 membrane with different loadings of HPA (2, 8, and 15 wt%) at 300 K. The major issue that is considered in this study is the role of POMs in morphology alternation and the changes created by them in two key proton transport mechanisms; namely, vehicular and hopping (Grotthuss) mechanisms.

From RDFs and coordination numbers, we first illustrated the morphological features of the membrane and described the behavior of solvent water and hydronium ions in the vicinity of sulfonic groups and around PW_{12} particles. It was concluded that fewer hydronium ions and fewer water molecules solvate the sulfonic groups for a higher concentration of PW_{12} and that the separation distance between sulfur atoms increases. Instead, larger water clusters, at a given water uptake, were formed by more solvation of hydrophilic PW_{12}.

As a major asset of our Q-HOP MD simulations, the effects of HPA doping level on the vehicular and hopping transports in hydrophilic domains of the Nafion were examined based on the lifetime of H-bonds. There are stronger hydrogen bond networks between water molecules and protons in pure Nafion 117 but the network stability is comparable with that of PW_{12} doped membrane at the same hydration level.

The self-diffusion coefficient of water was found to decrease and the proton diffusion increased with the addition of HPA at all the hydration levels, in agreement with other simulations models and experimental studies. The proton transport mechanism is found to be dependent on the hydration and the HPA concentration; furthermore, the high hydrophilicity of HPA causes less vehicular transport. In general, the results indicate that HPA particles significantly influence the proton transport in a hydrophilic pocket of Nafion 117 through proton hopping enhancement. Finally, this study demonstrates that raising the concentration of HPA leads to increased proton conductivity in the membrane of the fuel cell, in agreement with other experimental studies.

Acknowledgements

We acknowledge that part of the computation was performed on the HPC center of Ferdowsi University of Mashhad. We would like to thank Dr. Dolores Melgar of the Institute of Chemical Research of Catalonia (ICIQ) for her helpful advice improving this article.

Conflict of interest

The authors declare no conflict of interest.

Keywords: fuel cells · membranes · molecular dynamics · Nafion/phosphotunstic acid · proton transport

[1] A. Jayakumar, S. P. Sethu, M. Ramos, J. Robertson, A. Al-Jumaily, *Ionics* **2015**, *21*, 1–18.
[2] N. G. Moreno, M. C. Molina, D. Gervasio, J. F. P. Robles, *Renewable Sustainable Energy Rev.* **2015**, *52*, 897–906.
[3] O. Savadogo, *J. Power Sources* **2004**, *127*, 135–161.
[4] Y. Devrim, A. Albostan, *Int. J. Hydrogen Energy* **2015**, *40*, 15328–15335.
[5] R. K. A. M. Mallant, *J. Power Sources* **2003**, *118*, 424–429.
[6] M. Noorkami, J. B. Robinson, Q. Meyer, O. A. Obeisun, E. S. Fraga, T. Reisch, P. R. Shearing, D. J. Brett, *Int. J. Hydrogen Energy* **2014**, *39*, 1439–1448.
[7] A. M. Herring, *J. Macromol. Sci., Polym. Rev.* **2006**, *46*, 245–296.
[8] F. Meng, N. V. Aieta, S. F. Dec, J. L. Horan, D. Williamson, M. H. Frey, P. Pham, J. A. Turner, M. A. Yandrasits, S. J. Hamrock, A. M. Herring, *Electrochim. Acta* **2007**, *53*, 1372–1378.
[9] D. R. Vernon, F. Meng, S. F. Dec, D. L. Williamson, J. A. Turner, A. M. Herring, *J. Power Sources* **2005**, *139*, 141–151.
[10] C. Yang, S. Srinivasan, A. B. Bocarsly, S. Tulyani, J. B. Benziger, *J. Membr. Sci.* **2004**, *237*, 145–161.
[11] X. Tong, N. Tian, W. Wu, W. Zhu, Q. Wu, F. Cao, W. Yan, A. B. Yaroslavtsev, *J. Phys. Chem. C* **2013**, *117*, 3258–3263.
[12] E. Abouzari-lotf, M. M. Nasef, H. Ghassemi, M. Zakeri, A. Ahmad, Y. Abdollahi, *ACS Appl. Mater. Interfaces* **2015**, *7*, 17008–17015.
[13] A. I. Chikin, A. V. Chernyak, Z. Jin, Y. S. Naumova, A. E. Ukshe, N. V. Smirnova, V. I. Volkov, Y. A. Dobrovolsky, *J. Solid State Electrochem.* **2012**, *16*, 2767–2775.
[14] M. P. Allen, *Comput. Soft Matter: From Synthetic Polym. Proteins* (Ed.: N. Attig), NIC Series, **2004**, *23*, 1–28.
[15] G. M. Haugen, F. Meng, N. V. Aieta, J. L. Horan, M.-C. Kuo, M. H. Frey, S. J. Hamrock, A. M. Herring, *Electrochem. Solid-State Lett.* **2007**, *10*, B51–B55.
[16] V. Ramani, H. R. Kunz, J. M. Fenton, *J. Membr. Sci.* **2004**, *232*, 31–44.
[17] V. Ramani, H. R. Kunz, J. M. Fenton, *J. Membr. Sci.* **2005**, *266*, 110–114.
[18] V. Ramani, H. R. Kunz, J. M. Fenton, *Electrochim. Acta* **2005**, *50*, 1181–1187.
[19] S. Malhotra, R. Datta, *J. Electrochem. Soc.* **1997**, *144*, L23–L26.
[20] K.-D. Kreuer, *Chem. Mater.* **1996**, *8*, 610–641.
[21] Y. Liu, S. V. Sambasivarao, J. L. Horan, Y. Yang, C. M. Maupin, A. M. Herring, *J. Phys. Chem. C* **2014**, *118*, 854–863.
[22] H. Tian, O. Savadogo, *J. New Mater. Electrochem. Syst.* **2006**, *9*, 61.
[23] C. Arntsen, J. Savage, Y. L. Tse, G. Voth, *Fuel Cells* **2016**, *16*, 695–703.
[24] T. Mabuchi, T. Tokumasu, *J. Nanosci. Nanotechnol.* **2015**, *15*, 2958–2963.
[25] S. Liu, J. Savage, G. A. Voth, *J. Phys. Chem. C* **2015**, *119*, 1753–1762.
[26] M. A. Lill, V. Helms, *J. Chem. Phys.* **2001**, *115*, 7993–8005.
[27] W. Gu, T. Frigato, T. P. Straatsma, V. Helms, *Angew. Chem. Int. Ed.* **2007**, *46*, 2939–2943; *Angew. Chem.* **2007**, *119*, 2997–3001.
[28] W. Gu, V. Helms, *ChemPhysChem* **2007**, *8*, 2445–2451.
[29] B. L. de Groot, T. Frigato, V. Helms, H. Grubmüller, *J. Mol. Biol.* **2003**, *333*, 279–293.
[30] R. Devanathan, A. Venkatnathan, R. Rousseau, M. Dupuis, T. Frigato, W. Gu, V. Helms, *J. Phys. Chem. B* **2010**, *114*, 13681–13690.
[31] S. J. Paddison, J. A. Elliott, *J. Phys. Chem. A* **2005**, *109*, 7583–7593.
[32] S. S. Jang, V. Molinero, T. Çağın, W. A. Goddard, *J. Phys. Chem. B* **2004**, *108*, 3149–3157.
[33] T. Mabuchi, T. Tokumasu, *J. Chem. Phys.* **2014**, *141*, 104904.
[34] M. Levitt, M. Hirshberg, R. Sharon, K. E. Laidig, V. Daggett, *J. Phys. Chem. B* **1997**, *101*, 5051–5061.
[35] Gaussian 98, M. J. Frisch, G. W. Trucks, H. B. Schlegel, G. E. Scuseria, M. A. Robb, J. R. Cheeseman, V. G. Zakrzewski, J. A. Montgomery Jr., R. E. Stratmann, J. C. Burant, S. Dapprich, J. M. Millam, A. D. Daniels, K. N. Kudin, M. C. Strain, O. Farkas, J. Tomasi, V. Barone, M. Cossi, R. Cammi, B. Mennucci, C. Pomelli, C. Adamo, S. Clifford, J. Ochterski, G. A. Petersson,

P. Y. Ayala, Q. Cui, K. Morokuma, P. Salvador, J. J. Dannenberg, D. K. Malick, A. D. Rabuck, K. Raghavachari, J. B. Foresman, J. Cioslowski, J. V. Ortiz, A. G. Baboul, B. B. Stefanov, G. Liu, A. Liashenko, P. Piskorz, I. Komaromi, R. Gomperts, R. L. Martin, D. J. Fox, T. Keith, M. A. Al-Laham, C. Y. Peng, A. Nanayakkara, M. Challacombe, P. M. W. Gill, B. Johnson, W. Chen, M. W. Wong, J. L. Andres, C. Gonzalez, M. Head-Gordon, E. S. Replogle, J. A. Pople, Gaussian, Inc., Pittsburgh, PA, 1998..

[36] C. M. Breneman, K. B. Wiberg, *J. Comput. Chem.* **1990**, *11*, 361 – 373.

[37] X. López, C. Nieto-Draghi, C. Bo, J. B. Avalos, J. M. Poblet, *J. Phys. Chem. A* **2005**, *109*, 1216 – 1222.

[38] M. C. Payne, M. P. Teter, D. C. Allan, T. A. Arias, J. D. Joannopoulos, *Rev. Mod. Phys.* **1992**, *64*, 1045 – 1097.

[39] D. R. Morris, X. Sun, *J. Appl. Polym. Sci.* **1993**, *50*, 1445 – 1452.

[40] M. Allen, D. Tildesley, *Computer Simulation of Liquids*, Oxford University Press, New York, **1987**, Chap. 2.

[41] I. T. Todorov, W. Smith, K. Trachenko, M. T. Dove, *J. Mater. Chem.* **2006**, *16*, 1911 – 1918.

[42] H. J. C. Berendsen, J. P. M. Postma, W. F. van Gunsteren, A. DiNola, J. R. Haak, *J. Chem. Phys.* **1984**, *81*, 3684 – 3690.

[43] W. G. Hoover, *Phys. Rev. A* **1986**, *34*, 2499 – 2500.

[44] U. Essmann, L. Perera, M. L. Berkowitz, T. Darden, H. Lee, L. G. Pedersen, *J. Chem. Phys.* **1995**, *103*, 8577 – 8593.

[45] H. J. C. Berendsen, J. R. Grigera, T. P. Straatsma, *J. Phys. Chem.* **1987**, *91*, 6269 – 6271.

[46] E. J. Bylaska, W. A. De Jong, N. Govind, K. Kowalski, T. P. Straatsma, M. Valiev, D. Wang, E. Apra, T. L. Windus, J. Hammond, *PNNL*, *Richland, Washington.* **2007**, 99352: 0999.

[47] R. A. Kendall, E. Aprà, D. E. Bernholdt, E. J. Bylaska, M. Dupuis, G. I. Fann, R. J. Harrison, J. Ju, J. A. Nichols, J. Nieplocha, *Comput. Phys. Commun.* **2000**, *128*, 260 – 283.

[48] J. Wang, P. Cieplak, P. A. Kollman, *J. Comput. Chem.* **2000**, *21*, 1049 – 1074.

[49] J. Wang, R. M. Wolf, J. W. Caldwell, P. A. Kollman, D. A. Case, *J. Comput. Chem.* **2004**, *25*, 1157 – 1174.

[50] R. Devanathan, A. Venkatnathan, M. Dupuis, *J. Phys. Chem. B* **2007**, *111*, 8069 – 8079.

[51] A. Chaumont, G. Wipff, *Phys. Chem. Chem. Phys.* **2008**, *10*, 6940 – 6953.

[52] S. Cui, J. Liu, M. K. Selvan, D. J. Keffer, B. J. Edwards, W. V. Steele, *J. Phys. Chem. B* **2007**, *111*, 2208 – 2218.

[53] C. Nieto-Draghi, J. B. Avalos, B. Rousseau, *J. Chem. Phys.* **2003**, *118*, 7954 – 7964.

[54] K.-D. Kreuer, *Solid State Ionics* **2000**, *136*, 149 – 160.

[55] K.-D. Kreuer, S. J. Paddison, E. Spohr, M. Schuster, *Chem. Rev.* **2004**, *104*, 4637 – 4678.

[56] W. Humphrey, A. Dalke, K. Schulten, *J. Mol. Graphics* **1996**, *14*, 33 – 38.

[57] K.-D. Kreuer, T. Dippel, W. Meyer, J. Maier, *MRS Online Proceedings Library Archive* **1992**, *293*, 273 – 282.

[58] Y.-L. S. Tse, A. M. Herring, K. Kim, G. A. Voth, *J. Phys. Chem. C* **2013**, *117*, 8079 – 8091.

[59] J.-C. Perrin, S. Lyonnard, F. Volino, *J. Phys. Chem. C* **2007**, *111*, 3393 – 3404.

[60] T. A. Zawodzinski, M. Neeman, L. O. Sillerud, S. Gottesfeld, *J. Phys. Chem.* **1991**, *95*, 6040 – 6044.

[61] J. B. Moffat, *Polyhedron* **1986**, *5*, 261 – 269.

Manuscript received: June 28, 2017
Revised manuscript received: September 11, 2017
Accepted manuscript online: September 19, 2017
Version of record online: November 8, 2017